Acta Biomaterialia 8 (2012) 2047–2055

Contents lists available at SciVerse ScienceDirect

Acta Biomaterialia

journal homepage: www.elsevier.com/locate/actabiomat

Magnetic targeting of surface-modified superparamagnetic iron oxide nanoparticles yields antibacterial efficacy against biofilms of gentamicin-resistant staphylococci

Guruprakash Subbiahdoss [a], Shahriar Sharifi [a], Dirk W. Grijpma [a,b], Sophie Laurent [c], Henny C. van der Mei [a,*], Morteza Mahmoudi [d,e], Henk J. Busscher [a]

[a] Department of Biomedical Engineering, W.J. Kolff Institute, University Medical Center Groningen and University of Groningen, Antonius Deusinglaan 1, 9713 AV Groningen, The Netherlands
[b] Department of Biomaterial Science and Technology, University of Twente, P.O. Box 217, 7500 AE Enschede, The Netherlands
[c] Department of General, Organic, and Biomedical Chemistry, NMR and Molecular Imaging Laboratory, University of Mons, Avenue Maistriau, 19, B-7000 Mons, Belgium
[d] National Cell Bank, Pasteur Institute of Iran, #69 Pasteur Avenue, Tehran 13164, Iran
[e] Nanotechnology Research Center, Faculty of Pharmacy, Tehran University of Medical Sciences, Tehran, Iran

ARTICLE INFO

Article history:
Received 21 November 2011
Received in revised form 23 February 2012
Accepted 1 March 2012
Available online 8 March 2012

Keywords:
Superparamagnetic iron oxide nanoparticles
Magnetism
Surface functionalities
Biofilm

ABSTRACT

Biofilms on biomaterial implants are hard to eradicate with antibiotics due to the protection offered by the biofilm mode of growth, especially when caused by antibiotic-resistant strains. Superparamagnetic iron oxide nanoparticles (SPIONs) are widely used in various biomedical applications, such as targeted drug delivery and magnetic resonance imaging. Here, we evaluate the hypothesis that SPIONs can be effective in the treatment of biomaterial-associated infection. SPIONs can be targeted to the infection site using an external magnetic field, causing deep penetration in a biofilm and possibly effectiveness against antibiotic-resistant strains. We report that carboxyl-grafted SPIONs, magnetically concentrated in a biofilm, cause an approximately 8-fold higher percentage of dead staphylococci than does gentamicin for a gentamicin-resistant strain in a developing biofilm. Moreover, magnetically concentrated carboxyl-grafted SPIONs cause bacterial killing in an established biofilm. Thus magnetic targeting of SPIONs constitutes a promising alternative for the treatment of costly and recalcitrant biomaterial-associated infections by antibiotic-resistant strains.

© 2012 Acta Materialia Inc. Published by Elsevier Ltd. All rights reserved.

1. Introduction

The average life expectancy in the Western world is steadily increasing and is currently well over 70 years, both for men and women. With aging, the natural ability of the human body to restore function after trauma or wear is decreasing, while frequently also (oncological) intervention surgery, such as after total laryngectomy for the removal of a laryngeal tumour, yields loss of function as an unwanted side-effect. Biomaterial implants are indispensable in modern medicine for the restoration of function and allow large numbers of patients to maintain a high quality of life as they grow old. Infection of biomaterial implants or devices constitutes their major cause of failure and can develop many years after implantation [1]. Biomaterial-associated infection (BAI) can develop from perioperative bacterial contamination of implant surfaces during implantation, immediately post-surgery during hospitalization or by haematogenous spreading of bacteria from infections elsewhere in the body [2]. In general, *Staphylococcus epidermidis* and *Staphylococcus aureus* are the most frequently isolated pathogens from infected biomaterial implant surfaces. Almost 50% of infections associated with catheters, artificial joints and heart valves are caused by *S. epidermidis* [3], whereas *S. aureus* is detected in approximately 23% of infections associated with prosthetic joints [3].

The bacteria involved in BAI often protect themselves against antibiotics and the host immune system by producing a matrix of exopolymeric substances (Fig. 1A) that embeds the organisms and is impenetrable for most antibiotics and immune cells. Metals such as silver, copper, gold, titanium and zinc have been used as antibacterial agents for centuries, but their efficacy has been surpassed by modern antibiotics and their use has diminished. Since there is growing concern that the era of antibiotics may well come to an end over the coming decades and more and more multiple-antibiotic-resistant strains are arising, alternative strategies are badly needed especially against antibiotic-resistant strains [4]. Application of metals in their nanoparticulate form is currently

* Corresponding author. Tel.: +31 50 3633140; fax: +31 50 3633159.
E-mail address: h.c.van.der.mei@umcg.nl (H.C. van der Mei).

1742-7061/$ - see front matter © 2012 Acta Materialia Inc. Published by Elsevier Ltd. All rights reserved.
http://dx.doi.org/10.1016/j.actbio.2012.03.002

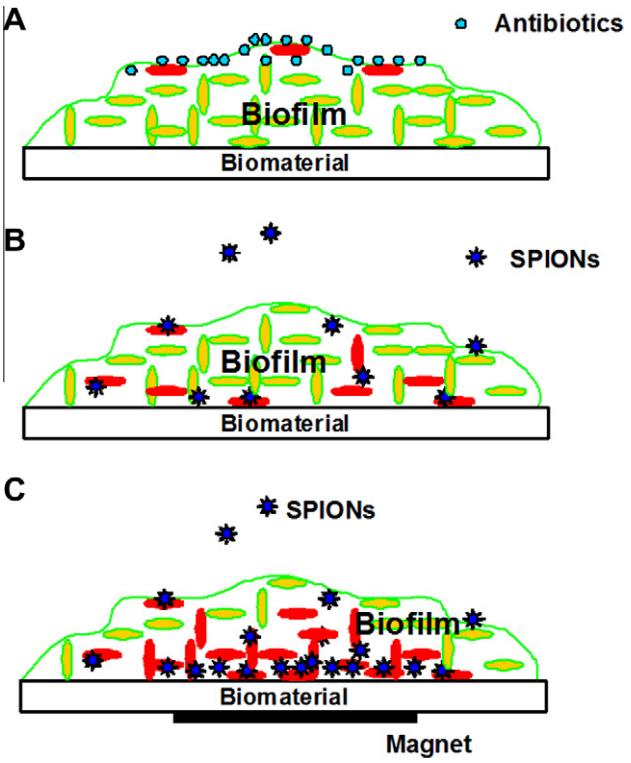

Fig. 1. The biofilm mode of bacterial growth on a biomaterial surface prevents the penetration of antibiotics into the biofilm (A), while it may allow penetration of SPIONs (B). An external magnetic field can facilitate deep penetration of SPIONs into the biofilm, and magnetic concentration in a region can enhance antibacterial efficacy (C). Red colour represents dead bacteria and green colour represents live bacteria.

being considered to resolve bacterial infections, but has attracted scientific attention only over the past decade [5]. Nanoparticles are less than 100 nm in diameter and, as a result, properties such as surface area, chemical reactivity and biological activity alter dramatically. The antibacterial efficacy of metal nanoparticles has been suggested to be due to their high surface area to volume ratio rather than to the sole effect of metal ion release [6]. A high surface area to volume ratio is generally accompanied by increased production of reactive oxygen species (ROS), including free radicals [7,8]. These characteristics allow nanoparticles to interact closely with microbial membranes, damage their structure and inactivate bacteria [5]. Metal oxide nanoparticles are of particular interest as antibacterial agents, as they can be prepared with extremely high surface areas and unusual crystalline morphologies with a high number of edges and corners, and other potentially reactive sites [9].

Superparamagnetic iron oxide nanoparticles (SPIONs) are a special class of metal oxide nanoparticles with unique magnetic properties and superior biocompatibility. Consequently, SPIONs have a wide history of application in the field of biomedical engineering, including their use as contrast agents for magnetic resonance imaging [10,11] and magnetic fluid hyperthermia [12], carriers for targeted drug delivery [13,14], magnetic separation of immune cells [15], proteins or other biomolecules [16] and tissue engineering applications [17,18]. Recently, Taylor et al. [19] proposed the use of superparamagnetic nanoparticles to prevent orthopaedic implant infection, showing that SPIONs in a concentration range of 0.01–2 mg ml^{-1} were able to kill up to 25% of *S. epidermidis* in a 48 h old biofilm [19]. Although the shape and size of SPIONs can contribute significantly to their antibacterial activity [20], specific surface chemical functionalities of SPIONs have also been suggested to be crucial to their interaction with bacterial cell membranes [21].

Here, we evaluate the hypothesis that SPIONs can be effective in the treatment of BAI (Fig. 1B), because they can be targeted to the infection site using an external magnetic field, causing deep penetration in a biofilm (Fig. 1C) and possibly effectiveness against antibiotic-resistant strains. First, we demonstrate the effects of surface-functionalized SPIONs (see Fig. 2) on soft tissue cells and on the viability of staphylococcal biofilms for a gentamicin-susceptible and -resistant strain, as compared with gentamicin, a frequently used antibiotic for treatment and prevention of prosthetic, orthopaedic joint infections. Next we demonstrate that magnetic targeting of SPIONs yields antibacterial efficacy against a developing and established biofilm of gentamicin-resistant staphylococci.

2. Materials and methods

2.1. Materials

$FeCl_2.4H_2O$, $FeCl_3.6H_2O$, diethylene glycol, 3-aminopropyltriethoxysilane (APTES), *o*-(2-aminoethyl)-*o*′-methylpolyethylene glycol (PEG-NH_2, MW = 750), *N*-(3-dimethylaminopropyl)-*N*′-ethylcarbodiimide hydrochloride, tetramethylammonium hydroxide, polyethylene glycol 8000 and *N*,*N*-dimethylformamide (DMF) were purchased from Sigma-Aldrich, Germany. Carboxyethylsilanetriol (CES) was provided by Wacker-Chemie GmbH, Burghausen, Germany.

2.2. Synthesis of SPIONs and grafting of surface functional groups

In order to obtain nanoparticles with a narrow size distribution, the polyol method was employed [22]. Briefly, 5 ml of an aqueous solution of $FeCl_2.4H_2O$ (0.045 M) and $FeCl_3.6H_2O$ (0.0375 M) were added to 250 ml of diethyleneglycol. The mixture was heated to 170 °C and maintained at this temperature for 15 min before addition of the base (i.e. solid NaOH until a final concentration of 0.375 M). Subsequently, temperature was maintained at 170 °C for a period of 1 h before cooling to 60 °C. The synthesized SPIONs were collected with a neodymium magnet and washed with 100 ml of a HNO_3 (1 M) solution.

Carboxyethylsilanetriol (CES) was grafted on the surfaces of SPIONs, as described elsewhere [23]. Briefly, 100 ml of nanoparticle solution (0.3 M iron) was added to 100 ml DMF and 45 ml of 0.15 M CES was slowly added before adding 25 ml water followed by 15 ml of NaOH solution (1 M) at room temperature and under homogenization (about 8000–24,000 rpm). The solution was heated to 100 °C for 24 h under continuous stirring. The SPIONs were precipitated by addition of acetone/ether (50/50) mixture and collected with a neodymium magnet. The precipitate was washed with acetone several times and finally dispersed in water. Excess of silane derivative and other chemicals were removed by dialysis using a dialysis bag (Spectrum Laboratories, Inc; MWCO = 10,000) for 48 h in water.

Aminopropyltriethoxysilane (APTES) was grafted onto SPIONs by first dissolving 15 ml of APTES in 50 ml methanol and subsequent dropwise addition to a suspension of nanoparticle solution (20 ml, [Fe] = 0.3 M) at room temperature. After stirring for 24 h at room temperature, 20 ml of glycerol was added to the mixture and subsequently methanol and water were removed by rotary evaporation. Next, 50 ml of acetone was added and, after mixing, the nanoparticles were separated by magnetic decantation. After removing the supernatant, SPIONs were washed several times with acetone. Afterwards, the magnetic nanoparticles were dispersed in 40 ml of water and purified by dialysis using a dialysis bag (MWCO = 10,000) for 48 h in water.

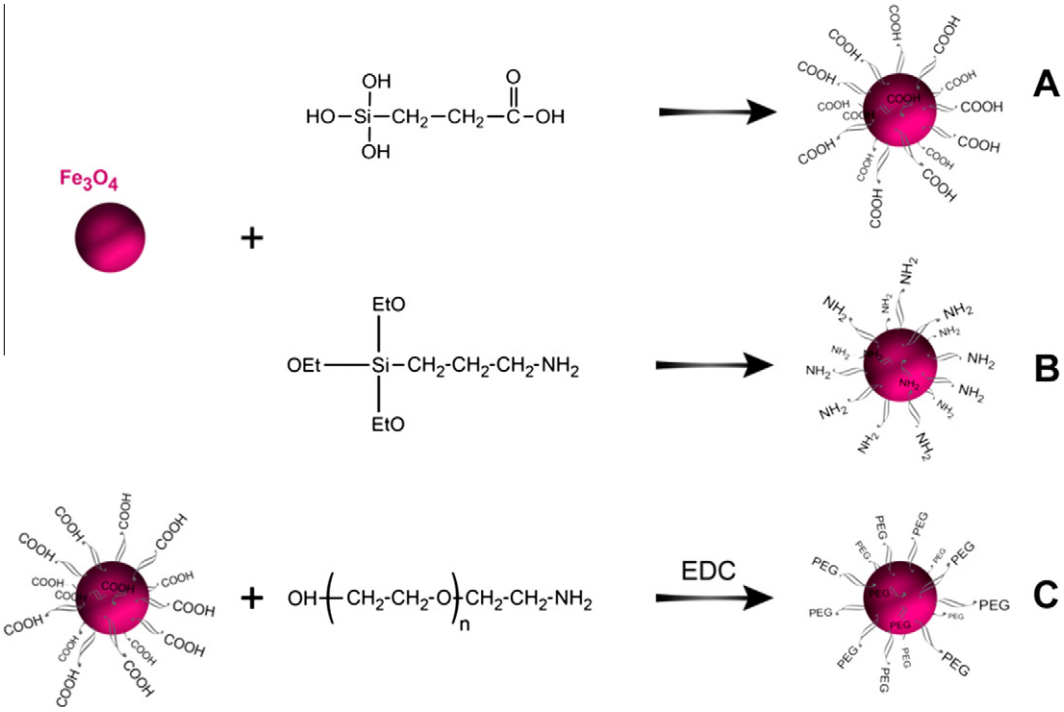

Fig. 2. Surface grafting of SPIONs with (A) carboxyl (CES), (B) amine (APTES) and (C) PEG functionalities (PEGylated).

PEGylation of SPIONs was done by an amidation reaction between aminopolyethylene glycol and carboxylic acid groups on the surface of CES-modified SPIONs. Briefly, 0.156 g of *N*-(3-dimethylaminopropyl)-*N*′-ethylcarbodiimide hydrochloride, as a carboxyl activator, and 0.254 g of PEG-NH_2 were added to 2 ml of Fe_3O_4-CES aqueous solution and the mixture was stirred at room temperature for 24 h and washed several times by ultrafiltration on a 30 kD membrane.

2.3. SPION characterization

Transmission electron microscopy (TEM) images of the SPIONs were taken on a Philips EM 420 (120 kV) and obtained by evaporating water from the dispersion on amorphous carbon-coated copper grids. The hydrodynamic diameters and zeta potentials of the SPIONs in water were measured using a Malvern Zeta Sizer Nano S-90 dynamic light scattering instrument. Fourier transform infrared (FTIR) spectra were obtained using a PerkinElmer Spectrum 100 spectrometer in the range of 4000–650 cm^{-1}, and each spectrum was obtained by averaging 32 interferograms with a resolution of 4 cm^{-1}. Samples for FTIR analysis were prepared by lyophilizing SPION suspensions in water and a thin film of lyophilized SPIONs was placed on the attenuated total reflectance crystal for spectral recording.

2.4. Mammalian cell growth in the presence of surface-modified SPIONs

U2OS osteosarcoma cells were routinely cultured in Dulbecco's modified Eagle's Medium low glucose supplemented with 10% fetal calf serum, and 0.2 mM of ascorbic acid-2-phosphate. U2OS cells were maintained in a T75 cell culture flask at 37 °C in a humidified 5% CO_2 atmosphere and harvested at 90% confluency using trypsin/ethylenediaminetetraacetic acid. Harvested cells were counted using a Bürker–Türk counting chamber and subsequently diluted to a concentration of 10^5 cells ml^{-1}.

To determine U2OS cell growth, 1 ml U2OS cell suspension was seeded into tissue culture polystyrene wells. After incubation at 37 °C in a humidified 5% CO_2 atmosphere for 12 h, SPIONs with different functionalities were added to the wells (0.35 mg ml^{-1}). Subsequently, cells were incubated at 37 °C in a humidified 5% CO_2 atmosphere for 24 h. After 24 h of incubation, the samples were prepared for immunocytochemical staining to assess U2OS cell morphology and spreading. For fixation, 2 ml of 3.7% formaldehyde in cytoskeleton stabilization buffer (0.1 M PIPES, 1 mM EGTA, 4% (w/v) polyethylene glycol 8000, pH 6.9) was added to the wells. Subsequently, cells were incubated in 0.5% Triton X-100 for 3 min, rinsed with phosphate-buffered saline (PBS; 10 mM potassium phosphate, 0.15 M NaCl, pH 7.0) and stained for 30 min with PBS containing DAPI and TRITC-phalloidin. Subsequently, cells were washed 4 times in PBS and examined by confocal laser scanning microscopy (CLSM; Leica DMRXE with a confocal TCS SP2 unit) with an HCX APO L 40.0 × 0.80 W objective and a HeNe 488/543/633 nm laser with an excitation filter of 543 nm and emission filter of 555–667 nm for TRITC and a UV laser with an excitation filter of 364 nm and emission filter of 400–550 nm for DAPI imaging. The images were obtained using sequential scanning with a step size of 1.0 μm. The number of adhering U2OS cells per unit area was determined using Scion image analysis software. For each surface-modified SPION, three images (375 × 375 μm) were randomly taken and analyzed. Experiments were performed in triplicate with separately cultured cells.

In order to visualize possible internalization of SPIONs by U2OS cells, samples were prepared for TEM. To this end, cells were fixed with 2.5% pentane-1,5-dial in a 0.1 M sodium cacodylate buffer (pH 7.4) and post-fixed in 1% osmium tetroxide. After a final wash with sodium cacodylate buffer, specimens were dehydrated through a graded series of ethanol baths (30–100%) and embedded in Epon resin. Ultrathin sections were cut using an ultramicrotome, transferred onto 200-mesh Cu TEM grids with Formvar support film, and stained with uranyl acetate and lead citrate for 15 min. Finally,

the samples were imaged with a Philips CM 100 transmission electron microscope.

2.5. Growth of adhering bacteria in the absence and presence of surface-modified SPIONs

Gentamicin-susceptible *S. aureus* ATCC 12600 and gentamicin-resistant *S. epidermidis* ATCC 35984 were used for this study. Staphylococci were first grown aerobically overnight at 37 °C on blood agar from a frozen stock. The plate was kept at 4 °C. For each experiment, one colony was inoculated in 10 ml of tryptone soy broth (TSB; OXOID, Basingstoke, UK) and cultured for 16 h. Bacteria were harvested by centrifugation at 5000*g* for 5 min at 10 °C and washed with sterile PBS. The bacteria are suspended in TSB to a concentration of 10^6 bacteria ml^{-1}.

Tissue culture polystyrene wells were filled with 1 ml of bacterial suspension in the absence or presence of SPIONs (0.35 mg ml^{-1}) with different functionalities. Bacteria were allowed to grow aerobically at 37 °C for 24 h. For gentamicin-resistant *S. epidermidis* ATCC 35984, additional experiments were done in the presence of 2 μg ml^{-1} gentamicin on tissue culture polystyrene wells using the above procedure.

Subsequently, wells were washed with PBS and unbound bacteria were removed. In order to assess the viability of adhering staphylococci after 24 h of biofilm growth, a vitality staining solution (3.34 mM SYTO 9 and 20 mM propidium iodide (Molecular Probes Inc., USA) in PBS) was added to the wells, after which the wells were incubated for 15 min in the dark at room temperature. For each type of SPION, three images (224 × 168 μm) were randomly taken using a fluorescence microscope (Leica DM4000B, Leica Microsystems GMBH, Germany). Next, the numbers of live and dead bacteria were determined using Scion image analysis software and data expressed as the percentage dead bacteria in the presence of the various surface-modified SPIONs. Experiments were performed in triplicate with separately cultured bacteria.

2.6. Magnetic targeting of CES-grafted SPIONs using external magnetic field during biofilm growth

In order to evaluate the effects of CES-grafted SPIONs on a developing biofilm, tissue culture polystyrene wells were filled with 1 ml of *S. epidermidis* ATCC 35984 suspension and allowed to adhere and grow aerobically at 37 °C for 24 h under the following conditions: (i) in the presence of CES-grafted SPIONs (0.35 mg/ml) with and without magnetic targeting; (ii) in the presence of gentamicin and CES-grafted SPIONs with and without magnetic targeting. Next, in order to evaluate the effect of CES-grafted SPIONs on an already established biofilm, tissue culture polystyrene wells were filled with 1 ml of *S. epidermidis* ATCC 35984 suspension and allowed to adhere and grow aerobically at 37 °C for 24 h. Then, CES-grafted SPIONs (0.35 mg ml^{-1}) were introduced with and without magnetic targeting. Thereafter, biofilms were allowed to grow for another 24 h. Subsequently, wells were washed with PBS and unbound bacteria were removed and the viability of adhering staphylococci, i.e. the percentage dead bacteria, was determined using Scion image analysis software as described above. Experiments were performed in triplicate with separately cultured bacteria.

2.7. Statistics

Statistical ANOVA analysis was performed, followed by a Tukey HSD post hoc test; a *P*-value of <0.05 was considered significant.

i

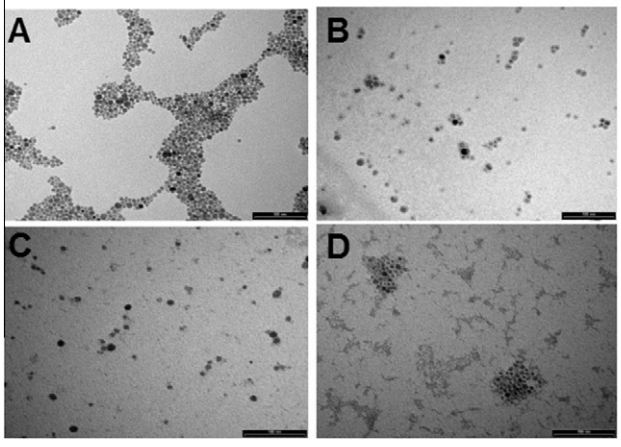

ii

SPIONs	Size (nm)	Zeta potential (mV)
Bare	13.7 ± 2.1	+43.7 ± 1.7
CES-grafted	13.8 ± 2.1	-15.4 ± 0.5
PEGylated	14.9 ± 1.8	-7.71 ± 0.9
APTES-grafted	17.8 ± 2.6	+32.6 ± 0.3

iii

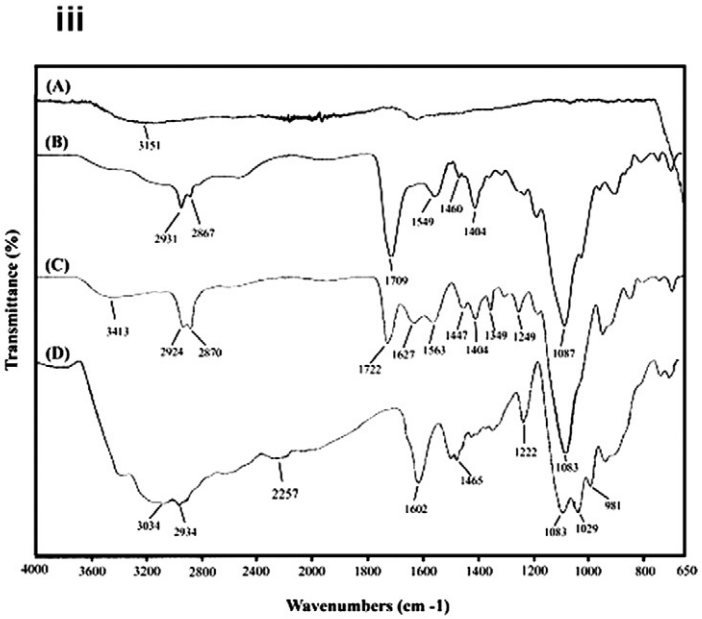

Fig. 3. (i) Transmission electron micrographs of (A) bare, (B) CES-grafted, (C) PEGylated and (D) APTES-grafted SPIONs. Bar denotes 100 nm. (ii) Diameters determined with dynamic light scattering and zeta potentials in water of the different surface-modified SPIONs, presented as mean ± SD over four samples. (iii) FTIR spectra of (A) bare, (B) CES-grafted, (C) PEGylated and (D) APTES-grafted SPIONs.

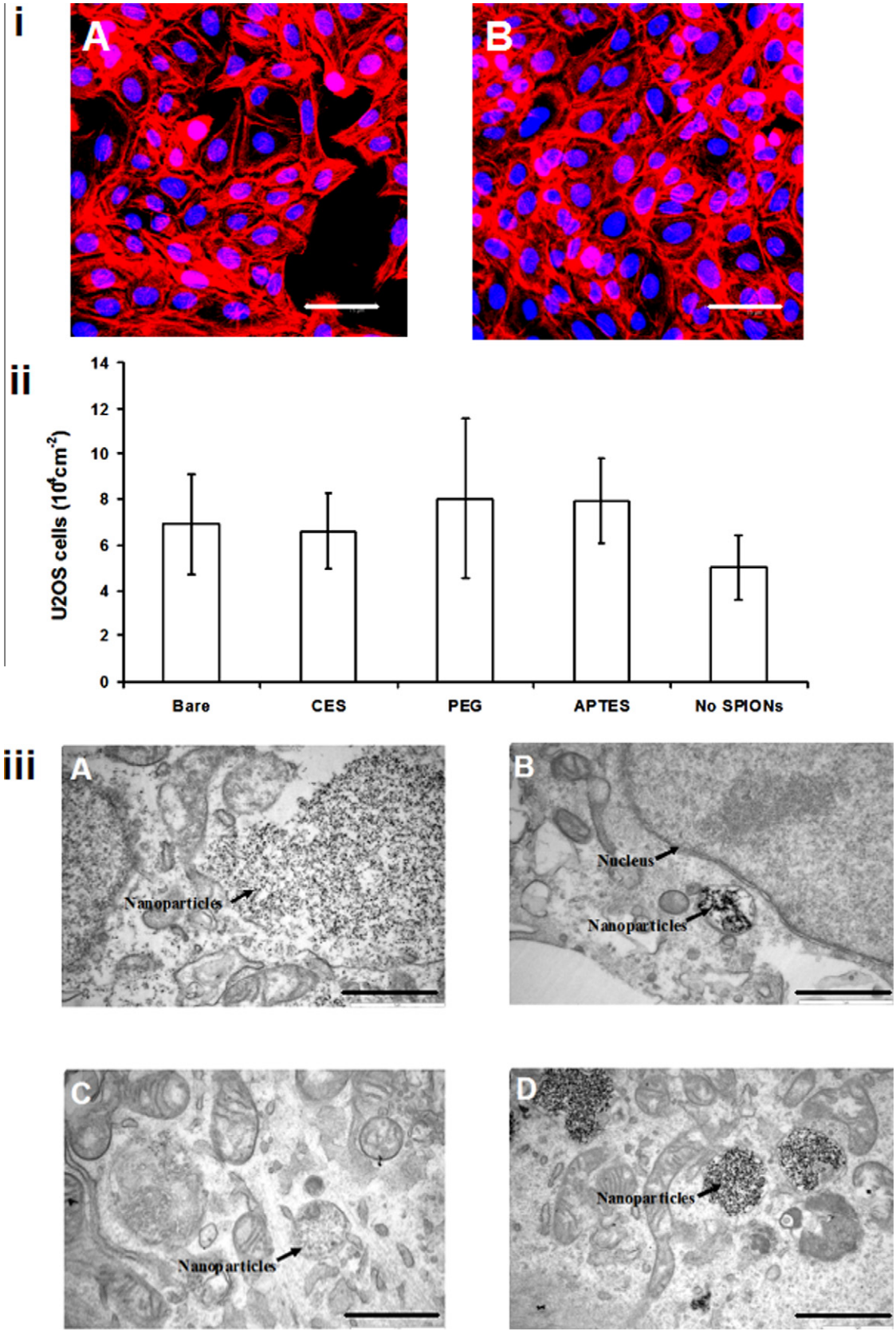

Fig. 4. (i) Confocal laser scanning microscopy images of U2OS cells after 24 h growth in tissue culture polystyrene wells: (A) absence of SPIONs; (B) presence of CES-grafted SPIONs. Bar denotes 75 μm. (ii) Number of U2OS cells after 24 h of growth in the presence of SPIONs. Error bars represents standard deviation over three independent experiments. (iii) Transmission electron micrographs of U2OS cells after 24 h of growth in tissue culture polystyrene wells in the presence of (A) bare, (B) CES-grafted, (C) PEGylated and (D) APTES-grafted SPIONs. Bar denotes 1 μm.

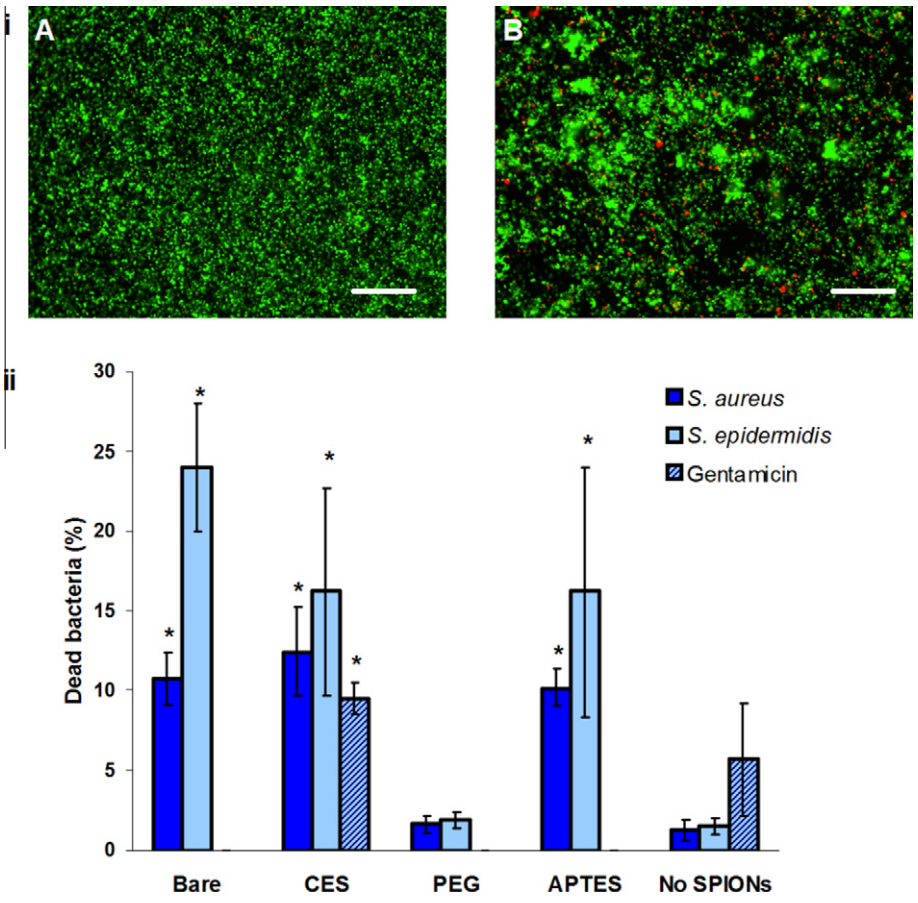

Fig. 5. (i) Fluorescence images of 24 h old *S. epidermidis* ATCC 35984 biofilms after live/dead staining in tissue culture polystyrene wells: (A) absence of SPIONs; (B) presence of CES-grafted SPIONs. Live and dead bacteria appear green and red fluorescent, respectively. Bar markers denote 25 μm. (ii) Percentage dead bacteria in 24 h old staphylococcal biofilms of *S. aureus* ATCC 12600 and *S. epidermidis* ATCC 35984 in the absence and presence of SPIONs. Error bars represent standard deviation over three independent experiments. Experiments with gentamicin were carried out on the gentamicin-resistant *S. epidermidis* ATCC 35984 with and without CES-grafted SPIONs. *Significantly different ($P < 0.01$) from data obtained in the absence of SPIONs.

3. Results and discussion

3.1. Characterization of SPIONs

TEM of the bare and surface-modified SPIONs are shown in Fig. 3i, confirming the formation of SPIONs with a very narrow size distribution. More quantitative size determinations are summarized in Fig. 3ii, together with the zeta potentials of the SPIONs in water. There are no significant differences in size of the various SPIONs, whereas the zeta potentials in water differ considerably. CES-grafted particles are negatively charged, while both bare and APTES-grafted SPIONs are positively charged. PEGylated SPIONs have a moderately negative surface charge. The FTIR spectrum of bare SPIONs (Fig. 3iii A) exhibited strong bands in the low-frequency region (750–400 cm^{-1}) due to the iron oxide skeleton [24,25]. The broad band at 3400–3500 cm^{-1} indicated the presence of surface hydroxyl groups. In the FTIR spectrum of CES-grafted SPIONs (Fig. 3iii B), a strong peak at 1709 cm^{-1} is present due to acidic carbonyl (C=O) groups [26]. Absorption bands at 2931 and 2867 cm^{-1} result from symmetric and asymmetric stretching vibrations of methylene groups in CES, respectively. C–O gives a very strong peak at 1087 cm^{-1}. The absorption band at 1460 cm^{-1} is due to bending vibrations of CH_2 groups. In addition, the stretching band of O–H groups can be seen around 3000 cm^{-1} as a broad band. By comparing the FTIR spectra of PEGylated SPIONs (Fig. 3iii C) with CES-grafted SPIONs, a successful covalent coupling of CES with PEG is confirmed. In the FTIR spectrum of PEGylated SPIONs, the intensity of C=O absorption band at 1710 cm^{-1} has decreased and a new band at 1627 cm^{-1} appears, which can be attributed to amide C=O groups. It shows that by the reaction of NH_2 groups of the PEG molecules with carboxylic acid groups on the nanoparticle surfaces, the number of carboxylic acid groups decreases and new C=O amide groups appear. As a result of the long chain of a PEG molecule and the methylene groups in the PEG structure, the intensity of stretching vibration of CH_2 (2924 and 2870 cm^{-1}) and the C–O band at 1063 cm^{-1} increase. In the FTIR spectrum of APTES-grafted SPIONs, the absorption band around 2934 cm^{-1} belongs to the stretching vibration of CH_2 groups. The stretching vibration of the C–N band has appeared at 1222 cm^{-1} and the band at 1465 cm^{-1} corresponds to the bending vibration of CH_2 groups. Furthermore, the broad band above 3000 cm^{-1} is due to N–H stretching, and the band at 1602 cm^{-1} belongs to the N–H bending vibration. FTIR analysis and zeta potentials thus demonstrate that post-synthesis surface modification of SPIONs through common silane-coupling compounds, such as APTES and CES [23], is a successful route to covalently bind organofunctionalities [27] to the SPION surface.

3.2. U2OS cell response in the presence of SPIONs

The response of U2OS cells after 24 h of growth in absence and presence of SPIONs is shown in Fig. 4. No differences in the U2OS

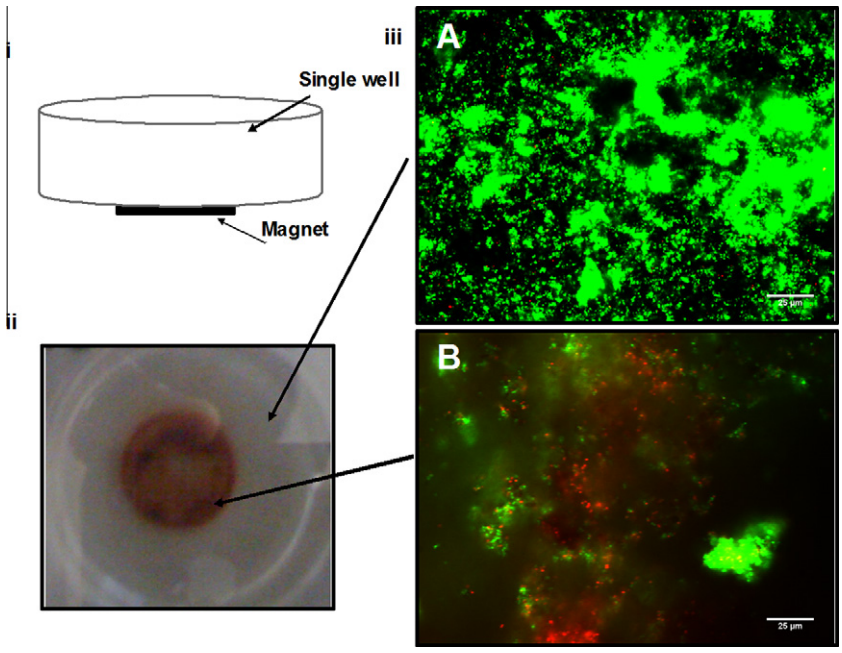

Fig. 6. Influence of magnetic directing of CES-grafted SPIONs in *S. epidermidis* ATCC 35984 biofilm. (i) Schematic presentation of the experimental set-up, showing a single well in which biofilms are grown in the absence or presence of SPIONs and positioning of a magnet underneath the well to target the SPIONs to a particular region of the biofilm. (ii) Top view of a tissue culture polystyrene well with a 24 h old *S. epidermidis* ATCC 35984 biofilm, showing magnetic concentration of SPIONs in the center of the well (red-dish area). (iii) Fluorescence image of 24 h old *S. epidermidis* ATCC 35984 biofilms after live/dead staining in tissue culture polystyrene wells: (A) for the area outside magnetic concentrating of CES-grafted SPIONs; (B) for the region where CES-grafted SPIONs were magnetically concentrated. Bar markers denote 25 µm.

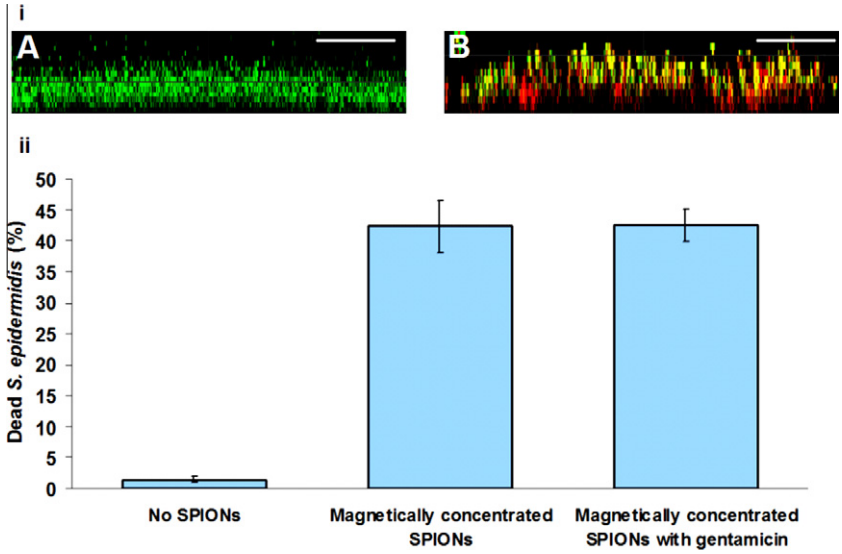

Fig. 7. (i) Optical cross-sections obtained using confocal laser scanning microscopy of 24 h old *S. epidermidis* ATCC 35984 biofilms after live/dead staining grown in (A) the absence of SPIONs; (B) the presence of magnetically concentrated CES-grafted SPIONs. Bar denotes 75 µm. (ii) Percentage of dead, gentamicin-resistant *S. epidermidis* ATCC 35984 in 24 h old biofilms, grown in the presence of magnetically directed CES-grafted SPIONs in the absence and presence of gentamicin. Error bars represents standard deviation over three independent experiments.

cell spreading and morphology (Fig. 4i) or cell number (Fig. 4ii) are observed between cells grown in the absence or presence of SPIONs. This indicates the absence of detrimental effects of SPIONs on U2OS cells.

SPIONs grafted with the PEG displayed minimal internalization (see Fig. 4iii C) due to their biological invisibility, and endocytosed PEGylated particles remain trapped in endolysosomal vesicles. Typically, incubation of nanoparticles with mammalian cells in media results in adsorption of serum proteins on their surfaces that induce the entry of nanoparticles into cells through receptor-mediated endocytosis. However, steric hindrance by hydrated and extended PEG-chains clearly prevent interaction of SPIONs with mammalian cells [28]. CES-grafted SPIONs are internalized in cells (Fig. 4iii B), despite the unfavourable electrostatic interaction between these particles and the negatively charged cell membrane, suggesting a role for ubiquitously present attractive Lifshitz–Van der Waals forces and clustering of the particles on scarcely distributed cationic sites on the cell membrane, resulting in their subsequent endocytosis [21]. Bare and APTES-grafted SPIONs are internalized in cells to a larger degree (Fig. 4iii A and D) than CES-grafted SPIONs due to their positive charge, yielding greater affinity for the mammalian cell membrane.

3.3. Antibacterial efficacy of surface-modified SPIONs against adhering staphylococci

In order to evaluate the hypothesis that SPIONs can be targeted to the infection site using an external magnetic field, causing deep penetration in a biofilm and acting effectively against antibiotic-resistant strains, we used a gentamicin-susceptible (*S. aureus* ATCC 12600) and gentamicin-resistant strain (*S. epidermidis* ATCC 35984). Fluorescent images of adhering *S. epidermidis* ATCC 35984 after 24 h of growth in the absence or presence of CES-grafted SPIONs are shown in Fig. 5i. The percentage dead bacteria in the biofilms (see Fig. 5ii) is significantly ($P < 0.01$) higher in the presence of bare, CES-grafted and APTES-grafted SPIONs than in their absence, both for *S. aureus* ATCC 12600 and gentamicin-resistant *S. epidermidis* ATCC 35984. Interestingly, PEGylated SPIONs showed no differences in the percentage of dead bacteria compared to the control for both strains. PEG is an amphiphilic polymer with highly mobile polymer chains that can attain extremely large exclusion volumes, hampering their interaction with bacteria and making them biologically "invisible".

The gentamicin resistance of *S. epidermidis* ATCC 35984 becomes evident from the observation that there is no significant difference in the percentage dead *S. epidermidis* in biofilms grown in the absence or presence of gentamicin (see also Fig. 5ii). Importantly, the presence of gentamicin and CES-grafted SPIONs causes a significant ($P < 0.05$) increase in the percentage of dead *S. epidermidis*, as compared with biofilms grown in the absence of SPIONs, which must be attributed solely to the SPIONs, and not to the gentamicin. In fact, the combined presence of gentamicin and CES-grafted SPIONs yields a statistically similar antibacterial efficacy as observed in the presence of SPIONs alone. These observations attest to the potential of SPIONs as an effective alternative to antibiotics in the fight against antibiotic-resistant strains.

3.4. Influence of magnetic targeting of CES-grafted SPIONs into a staphylococcal biofilm

CES-grafted SPIONs can be magnetically directed to become concentrated in a particular part of a biofilm (Fig. 6i and ii). Fluorescence images of a 24 h old biofilm of gentamicin-resistant *S. epidermidis* ATCC 35984 indicate a strong increase in the percentage of dead staphylococci in the region where CES-grafted SPIONs are magnetically concentrated (compare Fig. 6iii A and B).

Optical cross-sections of developing *S. epidermidis* biofilms grown in the absence of SPIONs and in the presence of magnetically targeted CES-grafted SPIONs are shown in Fig. 7i A and B, respectively. In the presence of magnetically targeted CES-grafted SPIONs, dead bacteria are observed in the bottom of the biofilm (see Fig. 7i B). Enumeration of the percentage of dead bacteria (Fig. 7ii) showed that magnetic targeting was much more efficient (44% dead bacteria) than the mere addition of SPIONs (16% dead bacteria). Note that the absence or presence of gentamicin did not affect bacterial killing by SPIONs of this gentamicin-resistant strain. Similar killing was observed when CES-grafted SPIONs were used to eradicate an established *S. epidermidis* biofilm, and whereas the presence of SPIONs only yielded 9% dead bacteria in the biofilm, magnetic targeting caused the death of around 38% of all bacteria in the biofilms (Fig. 8).

This is a unique effect, since biofilms show an inherent resistance to antimicrobial agents, such as antibiotics [29]. Antibiotics have difficulty penetrating an established biofilm because the biofilm matrix as produced by the microorganisms in the biofilm, adsorbs the antibiotics, resulting in the survival of organisms in the interior of the biofilm [29] and causing biofilm infections to become persistent. Another proposed mechanism for biofilm resistance against antimicrobial agents is that biofilm-associated organisms grow slowly, which makes them less susceptible to antimicrobial agents [30]. Physiological changes due to the biofilm mode of growth have been proposed as a mechanism as well [30]. Quantitatively, the percentage dead staphylococci in biofilms in the presence of magnetically concentrated CES-grafted SPIONs is significantly ($P < 0.01$) higher than in the absence of SPIONs, regardless of the absence or presence of gentamicin (Fig. 7ii). More importantly, and of major clinical relevance, magnetically concentrated CES-grafted SPIONs cause an approximately 8-fold higher percentage of dead staphylococci than does gentamicin for the gentamicin-resistant strain (compare Figs. 5 and 7ii). This confirms our hypothesis that SPIONs can be magnetically concentrated to yield antibacterial activity against antibiotic-resistant strains and provides a new and urgently needed strategy for the treatment of recalcitrant and costly biomaterial-implant-associated infections using magnetically targeted SPIONs.

The antibacterial activity of SPIONs could be due to several mechanisms. The main mechanism suggested is related to oxidative stress generated by ROS [31]. ROS includes superoxide radicals, hydroxyl radicals, hydrogen peroxide and singlet oxygen, that may cause chemical damage to proteins and DNA in bacteria [28]. In our study, bare, CES-grafted and APTES-grafted SPIONs showed similar antibacterial efficacy towards adhering staphylococci, including an antibiotic-resistant strain, which may suggest that the antibacterial activity of SPIONs is related to oxidative stress generated by ROS rather than the influence of specific

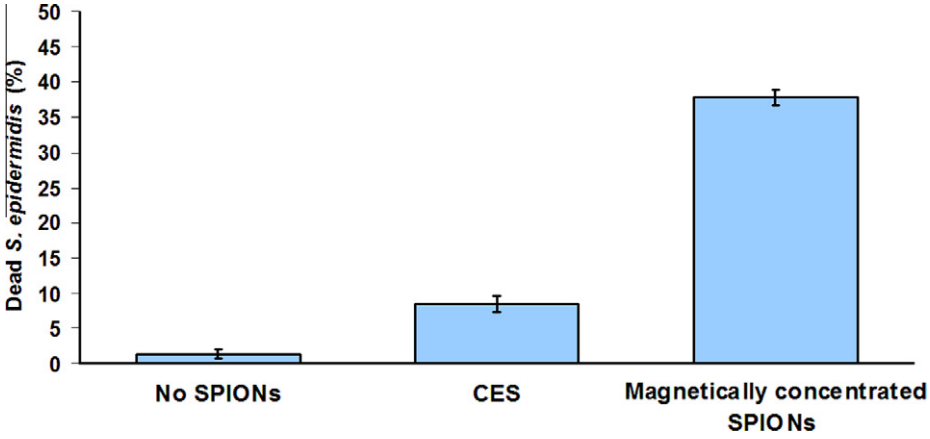

Fig. 8. Percentage of dead *S. epidermidis* ATCC 35984 in 48 h old biofilms, grown in the absence of CES-grafted SPIONs and after introducing CES-grafted SPIONs in an established 24 h old biofilm, followed by another 24 h of growth. SPIONs were introduced with and without magnetic targeting.

surface chemical functionalities. Secondly, electrostatic interactions between nanoparticles and bacterial cell membranes or cell membrane proteins can result in physical damage, which ultimately leads to bacterial cell death [31]. Although some studies showed that a positive charge on SPIONs is critical for their antibacterial efficacy [28,32], this study demonstrates a similar antibacterial efficacy for bare, CES-grafted and APTES-grafted SPIONs, regardless of the differences in zeta potentials measured in water. However, differences in zeta potentials are smaller in high ionic strength, physiological fluids, such as growth medium, resulting in a decrease in the influence of electrostatic interactions. This supports the above suggestion that the mechanism of antibacterial activity of SPIONs might be solely due to the creation of ROS via Fenton reactions leading to staphylococcal cell death [22]. Other studies demonstrated that the small size of nanoparticles could contribute to their antibacterial effects [23,27]. Lee et al. [33] reported that inactivation of *Escherichia coli* could be due to the penetration of nanoparticles with sizes ranging from 10 to 80 nm into *E. coli* membranes. Similarly, in our study the sizes of the nanoparticles are range from 14 to 18 nm and, based on their small size, bare, CES-grafted and APTES-grafted SPIONs could penetrate into the bacteria, leading to an increased percentage of dead bacteria. Simultaneously, PEGylated SPIONs are not efficient in killing adhering staphylococci compared to other surface-modified and unmodified SPIONs.

4. Conclusions

This study shows that surface-functionalized SPIONs can be used to kill staphylococci in their biofilm mode of growth. While no differences in antibacterial efficacy existed between bare, CES-grafted and APTES-grafted SPIONs, biologically, PEGylated SPIONs were ineffective against staphylococcal biofilms. None of the SPIONs were found to detrimentally affect mammalian cell adhesion and spreading, despite internalization by mammalian cells. PEGylated SPIONs, however, were also invisible to mammalian cells and were not internalized. An external magnetic field could target CES-grafted SPIONs into a biofilm of gentamicin-resistant staphylococci to yield a 8-fold higher antibacterial efficacy than gentamicin. Thus magnetic targeting of SPIONs into a biofilm constitutes a promising alternative for the treatment of costly and recalcitrant BAI by antibiotic-resistant strains.

Acknowledgement

This research was funded by the University Medical Center Groningen, Groningen, The Netherlands.

Appendix A. Figures with essential colour discrimination

Certain figures in this article, particularly Figs. 1, 2 and 4–8, are difficult to interpret in black and white. The full colour images can be found in the on-line version, at http://dx.doi.org/10.1016/j.actbio.2012.03.002.

References

[1] Costerton JW. Introduction to biofilm. Int J Antimicrob Agents 1999;11:217–21.
[2] Gristina AG. Biomaterial-centered infection: microbial adhesion versus tissue integration. Science 1987;237:1588–95.
[3] Khalil H, Williams RJ, Stenbeck G, Henderson B, Meghji S, Nair SP. Invasion of bone cells by *Staphylococcus epidermidis*. Microb Infect 2007;9:460–5.
[4] De Kraker MEA, Davey PG, Grundmann H. On behalf of the BURDEN study group. Mortality and hospital stay associated with resistant *Staphylococcus aureus* and *Escherichia coli* bacteremia: estimating the burden of antibiotic resistance in Europe. PLoS Med 2011;8:e1001104.
[5] Morones JR, Elechiguerra JL, Camacho A, Holt K, Kouri JB, Ramirez JT, et al. The bactericidal effect of silver nanoparticles. Nanotechnology 2005;16:2346–53.
[6] Allaker RP. The use of nanoparticles to control oral biofilm formation. J Dent Res 2010;89:1175–86.
[7] Nel AE, Madler L, Velegol D, Xia T, Hoek EMV, Somasundaran P, et al. Understanding biophysicochemical interactions at the nano-biointerface. Nat Mater 2009;8:543–57.
[8] Mahmoudi M, Lynch I, Ejtehadi MR, Monopoli MP, Bombelli F, Laurent S. Protein-nanoparticle interactions: opportunities and challenges. Chem Rev 2011;111:5610–37.
[9] Stoimenov PK, Klinger RL, Marchin GL, Klabunde KJ. Metal oxide nanoparticles as bactericidal agents. Langmuir 2002;18:6679–86.
[10] Mahmoudi M, Hosseinkhani H, Hosseinkani M, Boutry S, Simchi A, Journeay WS, et al. Magnetic resonance imaging tracking of stem cells in vivo using iron oxide nanoparticles as a tool for the advancement of clinical regenerative medicine. Chem Rev 2011;111:253–80.
[11] Amiri H, Mahmoudi M, Lascialfari A. Superparamagnetic colloidal nanocrystal clusters coated with polyethylene glycol fumarate: a possible novel theranostic agent. Nanoscale 2011;3:1022–30.
[12] Jordan A, Scholz R, Wust P, Fahling H, Felix R. Magnetic fluid hyperthermia (MFH): cancer treatment with AC magnetic field induced excitation of biocompatible superparamagnetic nanoparticles. J Magn Magn Mater 1999;201:413–9.
[13] Mahmoudi M, Sant S, Wang B, Laurent S, Sen T. Superparamagnetic iron oxide nanoparticles (SPIONs): development, surface modification and applications in chemotherapy. Adv Drug Delivery Rev 2011;63:24–46.
[14] Mahmoudi M, Milani AS, Stroeve P. Synthesis, surface architecture and biological response of superparamagnetic iron oxide nanoparticles for application in drug delivery: a review. Int J Biomed Nanosci Nanotechnol 2010;1:164–201.
[15] Mahmoudi M, Simchi A, Imani M. Recent advances in surface engineering of superparamagnetic iron oxide nanoparticles for biomedical applications. J Iran Chem Soc 2010;7:S1–S27.
[16] Horak D, Babic M, Mackova H, Benes MJ. Preparation and properties of magnetic nano- and microsized particles for biological and environmental separations. J Sep Sci 2007;30:1751–72.
[17] Ito A, Takizawa Y, Honda H, Hata KI, Kagami H, Ueda M, et al. Tissue engineering using magnetite nanoparticles and magnetic force. Heterotypic layers of cocultured hepatocytes and endothelial cells. Tissue eng 2004;10:833–40.
[18] Bock N, Riminucci A, Dionigi C, Russo A, Tampieri A, Landi E, et al. A novel route in bone tissue engineering: magnetic biomimetic scaffolds. Acta Biomater 2010;6:786–96.
[19] Taylor EN, Webster TJ. The use of superparamagnetic nanoparticles for prosthetic biofilm prevention. Int J Nanomed 2009;4:145–52.
[20] Mahmoudi M, Simchi A, Milani AS, Stroeve P. Cell toxicity of superparamagnetic iron oxide nanoparticles. J Colloid Interf Sci 2009;336:510–8.
[21] Verma A, Stellacci F. Effect of surface properties on nanoparticle-cell interactions. Small 2010;6:12–21.
[22] Forge D, Roch A, Laurent S, Tellez H, Gossuin Y, Renaux F, et al. Optimization of the synthesis of superparamagnetic contrast agents by the design of experiments method. J Phys Chem C 2008;112:19178–85.
[23] Xu ZH, Liu QX, Finch JA. Silanation and stability of 3-aminopropyl triethoxy silane on nanosized superparamagnetic particles: I. Direct silanation. Appl Surf Sci 1997;120:269–78.
[24] Bruce IJ, Taylor J, Todd M, Davies MJ, Borioni E, Sangregorio C, et al. Synthesis, characterisation and application of silica-magnetite nanocomposites. J Magn Magn Mater 2004;284:145–60.
[25] Wang L, Bao J, Wang L, Zhang F, Li Y. One-pot synthesis and bioapplication of amine-functionalized magnetite nanoparticles and hollow nanospheres. Chemistry 2006;12:6341–7.
[26] Das M, Mishra M, Maiti TK, Basak A, Pramanik P. Bio-functionalization of magnetite nanoparticles using an aminophosphonic acid coupling agent: new, ultradispersed, iron-oxide folate nanoconjugates for cancer-specific targeting. Nanotechnology 2008;19:415101.
[27] Laurent S, Forge D, Port M, Roch A, Robic C, Vander Elst L, et al. Magnetic iron oxide nanoparticles: synthesis, stabilization, vectorization, physicochemical characterizations, and biological applications. Chem Rev 2008;108:2064–110.
[28] Kim JS, Kuk E, Yu KN, Kim JH, Park SJ, Lee HJ, et al. Antimicrobial effects of silver nanoparticles. Nanomed-NBM 2007;3:95–101.
[29] Ishida H, Ishida Y, Kurosaka Y, Otani T, Sato K, Kobayashi H. In vitro and in vivo activities of levofloxacin against biofilm-producing *Pseudomonas aeruginosa*. Antimicrob Agents Chemother 1998;42:1641–5.
[30] Corbin A, Pitts B, Parker A, Stewart PS. Antimicrobial penetration and efficacy in an *in vitro* oral biofilm model. Antimicrob Agents Chemother 2011;55:3338–44.
[31] Li BK, Logan BE. Bacterial adhesion to glass and metal-oxide surfaces. Colloids Surf B 2004;36:81–90.
[32] El Badawy AM, Silva RG, Morris B, Scheckel K, Suidan MT, Tolaymat TM. Surface charge-dependent toxicity of silver nanoparticles. Environ Sci Technol 2011;45:283–7.
[33] Lee C, Kim JY, Lee WI, Nelson KL, Yoon J, Sedlak DL. Bactericidal effect of zero-valent iron nanoparticles on *Escherichia coli*. Environ Sci Technol 2008;42:4927–33.